Molecular taxonomy of human ocular outflow tissues defined by single-cell transcriptomics

Gaurang Patel[a,1], Wen Fury[a,1], Hua Yang[a], Maria Gomez-Caraballo[b], Yu Bai[a], Tao Yang[a], Christina Adler[a], Yi Wei[a], Min Ni[a], Heather Schmitt[b], Ying Hu[a], George Yancopoulos[a], W. Daniel Stamer[b,2], and Carmelo Romano[a,2]

[a]Regeneron Pharmaceuticals, Inc., Tarrytown, NY 10591; and [b]Department of Ophthalmology, Duke University, Durham, NC 27710

Edited by Joel S. Schuman, New York University, New York, NY, and accepted by Editorial Board Member Jeremy Nathans April 16, 2020 (received for review January 31, 2020)

The conventional outflow pathway is a complex tissue responsible for maintaining intraocular pressure (IOP) homeostasis. The coordinated effort of multiple cells with differing responsibilities ensures healthy outflow function and IOP maintenance. Dysfunction of one or more resident cell types results in ocular hypertension and risk for glaucoma, a leading cause of blindness. In this study, single-cell RNA sequencing was performed to generate a comprehensive cell atlas of human conventional outflow tissues. We obtained expression profiles of 17,757 genes from 8,758 cells from eight eyes of human donors representing the outflow cell transcriptome. Upon clustering analysis, 12 distinct cell types were identified, and region-specific expression of candidate genes was mapped in human tissues. Significantly, we identified two distinct expression patterns (myofibroblast- and fibroblast-like) from cells located in the trabecular meshwork (TM), the primary structural component of the conventional outflow pathway. We also located Schwann cell and macrophage signatures in the TM. The second primary component structure, Schlemm's canal, displayed a unique combination of lymphatic/blood vascular gene expression. Other expression clusters corresponded to cells from neighboring tissues, predominantly in the ciliary muscle/scleral spur, which together correspond to the uveoscleral outflow pathway. Importantly, the utility of our atlas was demonstrated by mapping glaucoma-relevant genes to outflow cell clusters. Our study provides a comprehensive molecular and cellular classification of conventional and unconventional outflow pathway structures responsible for IOP homeostasis.

glaucoma | trabecular meshwork | outflow facility | single-cell transcriptomics | anterior chamber

Elevated intraocular pressure (IOP) is a major causative risk factor for the development (1) and progression (2, 3) of most forms of glaucoma. Efficacious lowering of IOP, whether elevated or not, slows glaucomatous disease progression (2, 4). Current medical treatments lower IOP by three different mechanisms: suppressing aqueous humor formation, or increasing its rate of outflow via the unconventional or conventional outflow pathways (5, 6). While all three target tissues participate in aqueous humor dynamics, the conventional (trabecular) outflow pathway is responsible for homeostatically regulating IOP by the coordinated generation of outflow resistance involving cells that reside in the trabecular meshwork (TM) and Schlemm's canal (SC) (7–10). Importantly, dysfunction in the regulation of conventional outflow resistance results in elevated IOP in glaucoma patients (11, 12).

The TM is an avascular, complex connective tissue located at the iridocorneal angle, bridging from Schwalbe's line anteriorly to the scleral spur/ciliary muscle posteriorly. Anatomically, the TM is divided into three distinct tissue layers: the inner uveal meshwork, middle corneoscleral meshwork, and outer juxtacanalicular tissue (JCT, also known as cribriform tissue). Functioning as a biological filter, the uveoscleral and corneoscleral meshwork consists of collagen and elastin lamellae/plates covered by TM cells. In contrast, the JCT is composed of TM cells embedded in the extracellular matrix (ECM) of a loose connective tissue, directly interfacing with the inner wall of SC (reviewed in refs. 7 and 8). Cells that populate the TM are all of neural crest in origin (13), displaying different morphologies depending upon their tissue location. Thus, TM cells in uveal/corneoscleral meshwork display endothelial and macrophage properties, maintaining patent flow passageways by secreting antithrombotic molecules (14), phagocytosing cellular debris, neutralizing reactive oxygen species (15–17), and mediating immune function (18, 19), while the cells in the JCT region display fibroblast- and smooth muscle-like properties, playing an important role in the generation and control of outflow resistance (7). In response to various stimuli including mechanical cues (20–22), JCT cells continuously repair/remodel the ECM (23) and maintain contractile tissue tone in conjunction with the ciliary muscle. The importance of TM contractile tone in IOP regulation has been recently exploited pharmacologically by a new class of glaucoma drugs, the rho-kinase inhibitors, which selectively relax the TM and decrease outflow resistance (24).

Studies involving the use of TM and SC cells in cell and organ culture have resulted in the identification of multiple drug targets

Significance

Ocular hypertension is the primary and only modifiable risk factor for glaucoma, the leading cause of irreversible blindness. Intraocular pressure is regulated homeostatically by resistance to aqueous humor outflow through an architecturally complex tissue, the conventional/trabecular pathway. In this study, we generated a comprehensive cell atlas of the human trabecular meshwork and neighboring tissues using single-cell RNA sequencing. We identified 12 distinct cell types and mapped region-specific expression of candidate genes. The utility of our atlas was demonstrated by mapping glaucoma-relevant genes to conventional outflow cell types. Our study provides a comprehensive molecular and cellular classification of tissue structures responsible for intraocular pressure homeostasis in health and dysregulation in disease.

Author contributions: G.P., W.F., Y.H., G.Y., W.D.S., and C.R. designed research; G.P., W.F., H.Y., M.G.-C., H.S., and W.D.S. performed research; G.P., W.F., H.Y., M.G.-C., Y.B., T.Y., C.A., Y.W., M.N., Y.H., G.Y., W.D.S., and C.R. analyzed data; and G.P., W.F., Y.H., G.Y., W.D.S., and C.R. wrote the paper.

Competing interest statement: G.P., W.F., H.Y., Y.B., T.Y., C.A., Y.W., M.N., Y.H., G.Y., and C.R. are employees and shareholders of Regeneron Pharmaceuticals, although the manuscript's subject matter does not have any relationship to any products or services of this corporation.

This article is a PNAS Direct Submission. J.S.S. is a guest editor invited by the Editorial Board.

Data deposition: The raw data files from this study have been deposited in the Sequence Read Archive of the National Center for Biotechnology Information (accession no. PRJNA616025).

[1]G.P. and W.F. contributed equally to this work.

[2]To whom correspondence may be addressed. Email: dan.stamer@duke.edu or carmelo.romano@regeneron.com.

This article contains supporting information online at https://www.pnas.org/lookup/suppl/doi:10.1073/pnas.2001896117/-/DCSupplemental.

First published May 21, 2020.

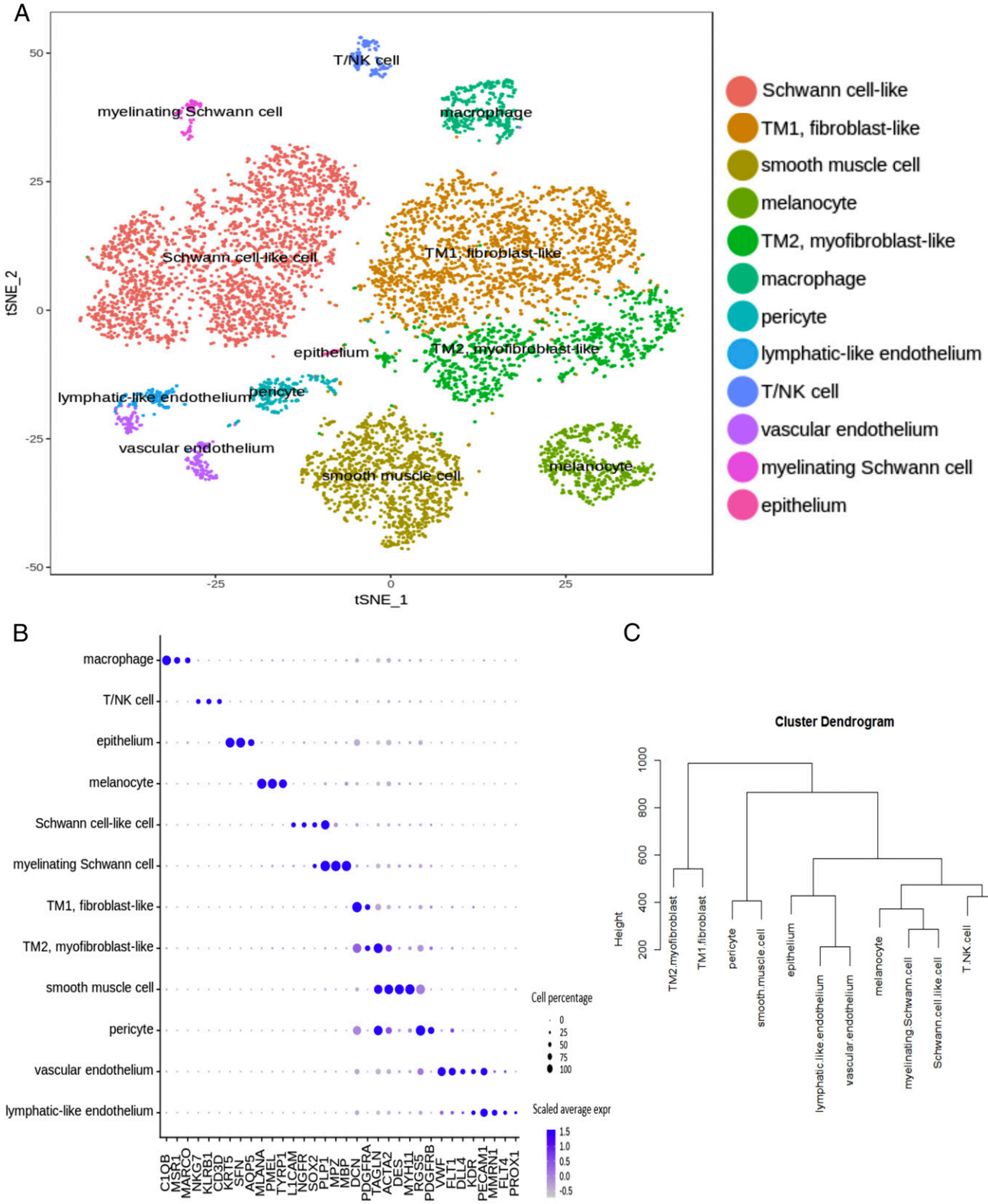

Fig. 1. Identification of human outflow cell types. (*A*) A *t*-distributed stochastic neighbor embedding (tSNE) visualization of outflow tissue transcriptome heterogeneity of 8,758 cells. Twelve distinct cell clusters were identified in the outflow tract, and cells are colored and labeled by cluster assignments. (*B*) Dot plot of gene expression combinations that uniquely identified each of the cell clusters. Quality control metrics are described in *Materials and Methods*. The size of each circle is proportional to the percentage of cells expressing the gene (marker) and its intensity depicts the normalized average transcript count of all cells within the cluster. (*C*) Hierarchical clustering of cell types, showing similarity or dissimilarity among cell types.

that are in various stages of clinical development, including rho-kinase inhibitors (25). However, due to their multiple responsibilities and unique environment, specific markers have not been identified for conventional outflow cells. Instead, cell morphology, growth characteristics, behavior, dissection technique, and a panel of protein markers are used for their identification and characterization. A typical panel of markers used to identify TM cells includes chitinase-3 like-1 (CHI3L1), matrix GLA protein (MGP), aquaporin-1 (25–28), and glucocorticoid-induced up-regulation of myocilin (MYOC) (29). Several transcriptomic and proteomic studies have been conducted to identify marker proteins; however, they were all based upon bulk tissue preparations that failed to identify cell-specific markers (30–35).

Recent advances in single-cell RNA sequencing (scRNAseq) allow molecular separation of different cell populations based on expression profiles at the single-cell level (36, 37). Such studies have been conducted using ocular tissues of the whole retina (38–40) and limbal/corneal epithelial tissues (41) but not outflow tissues. Like the retina, outflow tissues are ideal to study at the single-cell level because of their complex architecture and variety of cell types. Significantly, the critical role that TM and SC cells play in outflow resistance/IOP regulation and their accessibility for therapeutic interventions make them attractive targets for gene therapy for both congenital and adult forms of glaucoma. Moreover, identification of TM/SC cell-specific expression of proteins is critical for the identification of tissue-specific promoters needed for mechanistic studies involving transgenic/knockout mice.

To address these current deficiencies holding back glaucoma research, we performed scRNAseq of outflow tissues from human donor eyes and have identified cells in human outflow tissues that have 12 unique molecular signatures. Locations of cells having these RNA profiles were mapped using in situ hybridization and immunohistochemistry of human eye tissue. Taken together, this study provides a comprehensive molecular and cellular classification of conventional and unconventional outflow pathway tissues responsible for IOP regulation.

Results

Single-Cell Transcriptome Atlas of Human Outflow Cell Types. To generate an atlas of human conventional outflow tissues, we isolated TM tissue from eight different human donor eyes using a blunt dissection (*SI Appendix*, Fig. S1) and subjected the dissected tissue to enzymatic digestion to prepare a single-cell suspension. As reflected in *SI Appendix*, Fig. S1, there was a portion of the ciliary muscle and scleral spur region included in the dissection. Single-cell suspensions were checked for cell viability, with cells from four donor pairs (eight samples) included in subsequent droplet-based scRNAseq using the 10x Genomics platform (https://www.10xgenomics.com/). Unique molecular identifiers (UMIs) are molecular tags that are used to detect and quantify unique messenger RNA (mRNA) transcripts (source: https://www.illumina.com/). The average total UMIs detected was 4,516 (*SI Appendix*, Figs. S2*A* and S3*A*). The average gene count was 1,495 (*SI Appendix*, Figs. S2*B* and S3*B*) and the average mitochondrial read count percentage was 9.5% (*SI Appendix*, Figs. S2*C* and S3*C*). After the quality control metrics described in *Materials and Methods* were applied, we obtained 8,758 cells with 17,757 genes in total. The cells then were subjected to clustering analysis using Seurat 2.3 software and 12 clusters were identified. The cell identities were discovered by using cluster-specific genes as well as canonical cell-type markers (Fig. 1 *A* and *B*). From the most abundant to the least, cell signatures included Schwann cell-like, TM1 fibroblast-like, smooth muscle cell, TM2 myofibroblast-like, melanocyte, macrophage, pericyte, vascular endothelial cell, T cell/natural killer cells (T/NK), lymphatic-like endothelial cell, myelinating Schwann cell, and epithelial cell clusters (*SI Appendix*, Table S2). Each of the human TM samples contributed uniformly to all clusters (*SI Appendix*, Fig. S4), except for lymphatic-like endothelial cells and epithelial cells, which had low percentages in the overall cell population (1.42 and 0.34%, respectively). The percentage of cells in each cluster is registered in *SI Appendix*, Table S2. To better characterize each cell type, we studied the similarity and dissimilarity of the cell types by using the average UMIs of each gene across all cells within the same cell type for hierarchical clustering analysis. As expected, our results indicate that TM1 fibroblast-like and TM2 myofibroblast-like cells are similar to each other. Likewise, macrophages were similar to T/NK cells, pericytes shared likeness with smooth muscle, and vascular resembled lymphatic endothelial cells. Lastly, melanocytes, which could derive from Schwann cells during development, are similar to Schwann cells or Schwann cell-like cells (Fig. 1*C*).

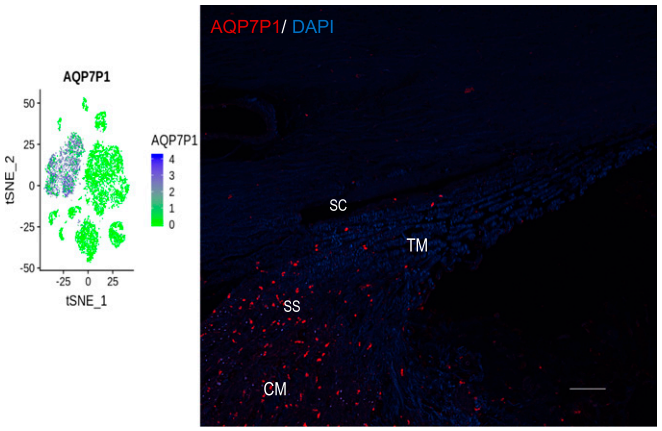

Fig. 2. In situ hybridization mapping of cells from the Schwann cell-like cluster in human eye sections. (*Left*) A tSNE plot showing normalized expression of the AQP7P1 gene in each cell (blue dots) is displayed. (*Right*) An in situ hybridization (ISH)-stained human eye section showing mRNA signal (red fluorescence) from the AQP7P1 gene. An mRNA probe corresponding to AQP7P1 predominantly localized to the scleral spur and ciliary muscle regions, with some cells extending into the TM. DAPI staining (blue) counterstains cell nuclei. Magnification, 20×. CM, ciliary muscle; SS, scleral spur. The scale in the tSNE plot shows the intensity of the natural log-transformed scaled read counts. (Scale bar, 50 μm.)

Characterization and Localization of Cluster-Specific Cell Markers in Human TM by RNAscope. We found genes that were enriched and sometimes specific to each cluster beyond canonical cell type-specific markers. To locate each of the clusters identified by scRNAseq in human outflow tissues, we performed RNAscope with different gene-specific probes. For identifying Schwann cell-like clusters, we selected RNA probes selective for aquaporin 7 pseudogene 1 (AQP7P1) (Fig. 2) and sodium voltage-gated channel alpha subunit 7 (SCN7A) (*SI Appendix*, Fig. S5). These markers localized to scleral spur and ciliary muscle regions. We observed that decorin (DCN) (Fig. 3*A*) and platelet-derived growth factor receptor alpha (PDGFRA) (Fig. 3*B*) were highly enriched in the TM1 fibroblast cell cluster but interestingly localized to several tissues including the scleral spur and JCT and SC regions of the TM. Although, R-spondin-4 (RSPO4) was specific to TM2 myofibroblast-like cluster and R-spondin-2 (RSPO2) was present in both TM1 and TM2 clusters, both cell types were found anatomically throughout TM.

We found the smooth muscle cluster gene muscle myosin heavy chain 1 (MYH11) (Fig. 5) was limited to the ciliary muscle region. Transgelin (TAGLN) (*SI Appendix*, Fig. S6) was highly enriched in TM2 and the smooth muscle cluster, correspondingly localized to both TM and ciliary muscle. Lymphatic vessel endothelial hyaluronan receptor 1 (LYVE1) (Fig. 6*A*), C1QB (Fig. 6*B*), and TYRO protein tyrosine kinase-binding protein (TYROBP)

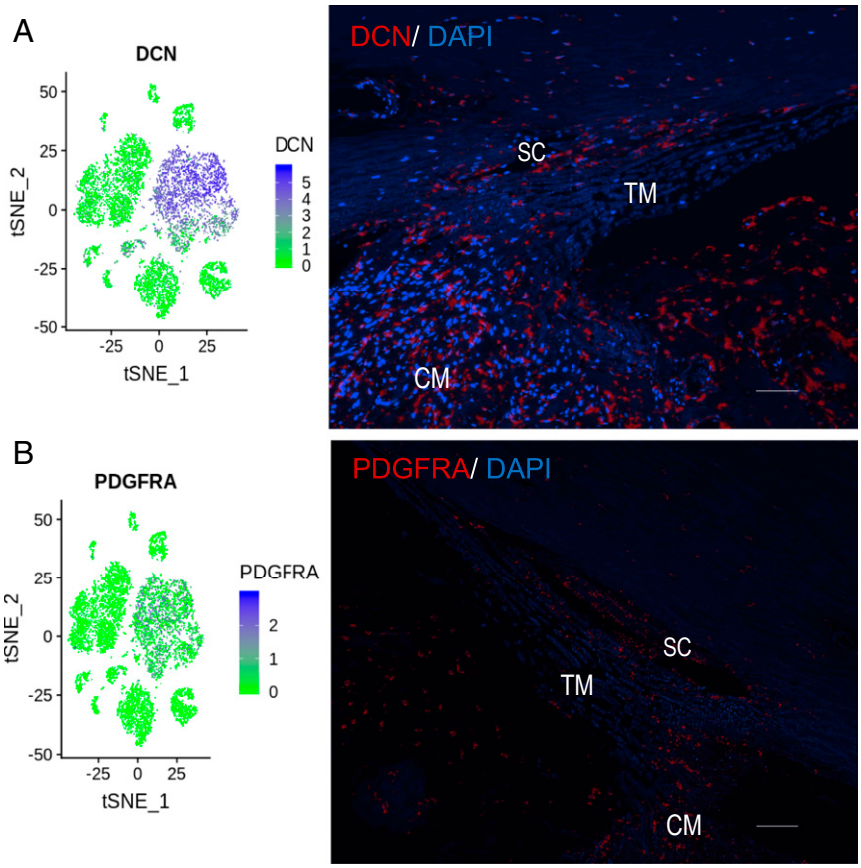

Fig. 3. Localization of TM1 fibroblast-like cell clusters using in situ hybridization of human eye sections. (*Left*) A tSNE plot of normalized gene expression in each cell (blue dots). (*Right*) An ISH-stained human eye section mapping mRNA signal as red fluorescence. mRNA probes specific for cluster markers DCN (*A*) and PDGFRA (*B*) were localized predominantly to JCT and SC regions of the conventional tract; however, scleral spur cells were also labeled. DAPI staining (blue) counterstains cell nuclei. Magnification, 20×. The scale in the tSNE plots shows the intensity of the natural log-transformed scaled read counts. (Scale bars, 50 μm.)

(*SI Appendix*, Fig. S7) were highly enriched in the macrophage cluster, and RNAscope revealed focal, macrophage-like labeling spread throughout the conventional outflow pathway. These results show that only three of the bioinformatically identified cell types (TM1, TM2, and macrophages) are found in the anatomically defined TM, and the others reflect cells from neighboring tissues (i.e., the unconventional outflow pathway).

Lymphatic-Like Endothelial Cell Cluster Has Both Lymphatic and Vascular Endothelial Phenotypes. Schlemm's canal plays an important role in IOP regulation via synergistic interaction with JCT cells (24, 42). SC is a unique structure displaying both blood vascular and lymphatic characteristics (43). Our scRNAseq data confirm these findings, with our transcriptome atlas showing a lymphatic-like endothelial cluster. Upon in-depth analysis, we found that this cluster expressed markers for both vascular and lymphatic endothelial-like cells (Fig. 7). Fms related receptor tyrosine kinase 4 (FLT4), fibronectin (FN1), and FLT1 (Fig. 8 and *SI Appendix*, Fig. S8) were expressed in the lymphatic-like and vascular endothelial cells and were all found to be in the SC region. Although FN1 and FLT1 were highly expressed in lymphatic-like endothelial and vascular endothelial clusters, respectively, they were also present in other clusters. FN1 was localized more to SC and JCT regions and enriched in scleral blood vessels. FLT1 was localized more in SC and ciliary muscle. In addition, our single-cell transcription analysis also provided the expression profiles of these unique cells at the whole-genome transcriptome level.

Cell Type-Specific Expression of Glaucoma-Related Genes. There are many genes that are implicated or associated with elevated IOP and glaucoma. We selected a few to see in which cell cluster they were present (Fig. 9*C* and Table 1). Mutations in MYOC cause glaucoma and angiopoietin-like 7 (ANGPTL7) (Fig. 9 *A* and *B*) is elevated in the aqueous humor of glaucoma patients (44–46). MYOC was highly expressed in TM1, TM2, and smooth muscle clusters and was expressed at high levels in the TM and at lower levels in ciliary muscle, SC, and scleral fibroblasts. Similarly, ANGPTL7 was found in both TM1 and TM2 clusters, but its expression was more limited, localizing to JCT and SC regions. Polymorphisms in a locus containing two genes, caveolins CAV1 and CAV2, are also implicated in elevated IOP and glaucoma (47, 48). In our scRNAseq outflow transcriptome, CAV1 and CAV2 were present in various different clusters including lymphatic-like and vascular endothelial, pericyte, smooth muscle cell, myelinating Schwann cell, melanocyte, and epithelial cell clusters (Fig. 9*C*). Interestingly, CAV1 and CAV2 were expressed at low levels in TM1 and TM2 but highly expressed in lymphatic-like and vascular endothelia cell clusters (i.e., SC). Autotaxin (gene name, ENPP2) has been shown to be elevated in the aqueous humor of glaucoma patients (49, 50) and studies have shown that autotaxin inhibitors lower IOP in mice and rabbits (49, 51). In the outflow transcriptome, ENPP2 was expressed in Schwann cell-like and melanocyte cell clusters (Fig. 9*C*). Polymorphisms in the gene encoding the endothelial-specific isoform of nitric oxide synthase (NOS3) gene encoding the endothelial-specific isoform of nitric oxide synthase (NOS) impart risk for ocular hypertension and glaucoma (52–55). Data here show that, indeed, NOS3 expression in the

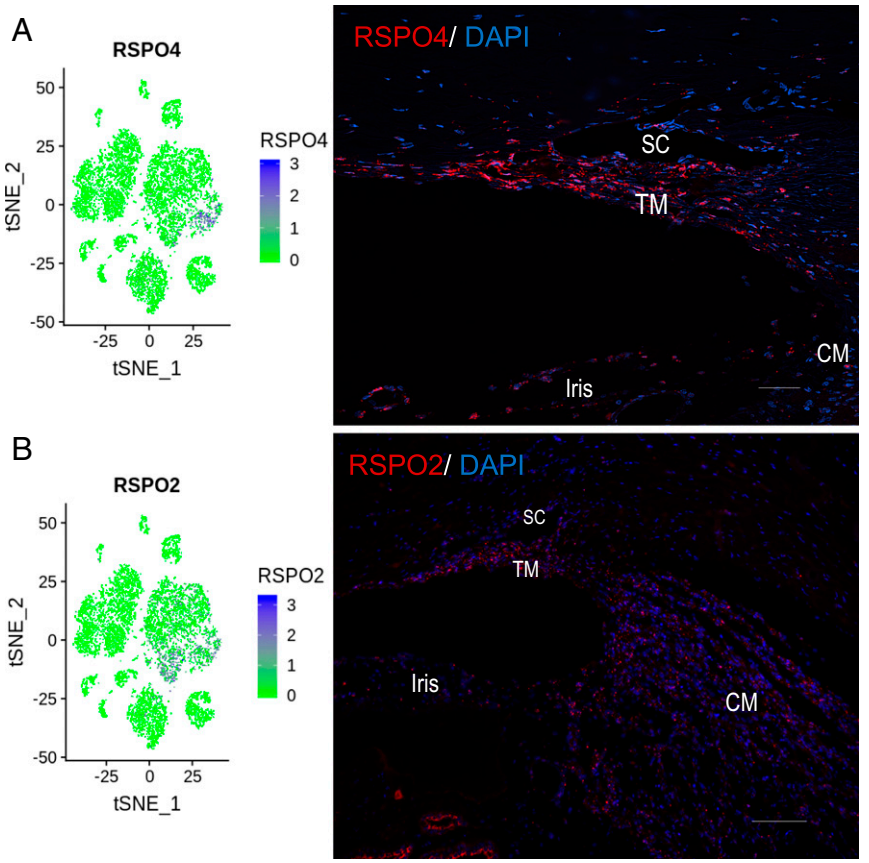

Fig. 4. Mapping of gene candidates from the TM2 myofibroblast-like cell cluster using in situ hybridization of human eye sections. (*Left*) A tSNE plot showing normalized expression of a gene in each cell (blue dots). (*Right*) An ISH-stained human eye section showing mRNA signal as red fluorescence. mRNA probes to candidates RSPO4 (*A*) and RSPO2 (*B*) were tested. RSPO4 expression was spread throughout the TM but not surrounding tissues, whereas RSPO2 expression was localized throughout the TM and neighboring tissues. DAPI staining (blue) counterstains cell nuclei. Magnification, 20× (*A*) and 10× (*B*). The scale in the tSNE plots shows the natural log-transformed scaled read counts. (Scale bars, 50 μm [*A*] and 100 μm [*B*].)

conventional outflow tract is confined to lymphatic-like and vascular endothelial cell clusters.

Both Tie2 and Angpt1 loss-of-function variants are associated with risk of congenital glaucoma, and single-nucleotide polymorphisms in the Angpt1 promoter region significantly associate with primary open-angle glaucoma risk (56–58). Consistent with immunofluorescence data in mice (59, 60), our scRNAseq data show that expression of Angpt1 in the conventional outflow tract is limited to TM cell clusters, while Tek (Tie2) and its antagonist, Angpt2, are expressed by lymphatic-like and vascular endothelial cell clusters. Many studies have described the use of CHI3L1, MGP, aquaporin-1, and αB-crystallin (CRYAB) (7, 25–28, 61) as markers to identify TM cells. In our scRNAseq transcriptome, CHI3L1 was confined to TM2 and TM1 cell clusters, MGP was localized to all cell clusters with more preference for TM1 and TM2 cell clusters, AQP1 was confined to TM2 and smooth muscle cell clusters, and CRYAB was localized to all cell clusters with more preference for Schwann cell-like, TM2, smooth muscle cell, melanocyte, and myelinating Schwann cell clusters. TM cells in uveal/corneoscleral meshwork secrete antithrombotic molecules (14) such as tissue plasminogen activator (PLAT), which helps in maintaining a clear passage for aqueous humor through TM and SC regions. The expression of PLAT was primarily localized to lymphatic-like and vascular endothelial and Schwann cell-like cell clusters, with some TM1 and TM2 expression. Podoplanin (PDPN, also known as D2-40) has been widely used as a marker to detect lymphatic vessels and studies have reported that TM stains positive for D2-40 in histological sections (62). Consistent with this finding, in our scRNAseq, PDPN was confined to TM1 and TM2 cell clusters but not the lymphatic-like and vascular endothelial cell clusters (Schlemm's canal).

Immunohistochemical Localization of Candidate Gene Products in Human Outflow Tissues. The protein products of select candidate genes identified by scRNAseq (*SI Appendix*, Table S3) were screened in sections of human outflow tissues. We focused on the four main cell types in the conventional outflow pathway: TM1, TM2, SC, and macrophages. A positive control for TM1 and TM2 was the glaucoma-related gene product myocilin, which labeled strongly in all regions of the TM and has weaker labeling in surrounding tissues (Fig. 10*A*). The vascular endothelial marker PECAM1 (CD31) was used to selectively label SC as a positive control (Fig. 10*B*). We tested a number of commercially available antibodies at different concentrations against gene candidates, using two different tissue preparation techniques on different donor eye sections (*SI Appendix*, Tables S3 and S4). We were unable to obtain specific labeling with a number of these antibodies; however, we reliably observed labeling with the TM1 candidate gene product RSPO2 (Fig. 10*C*). The labeling pattern was similar to that found with RNAscope (Fig. 4), labeling both TM1 and TM2 cells, with preference for JCT (TM1 cells). We also tried a number of different antibodies against SC candidates including endothelial nitric oxide synthase, VEGF receptor-3, trefoil factor-3, and TMEM88, but labeling was found to be nonspecific or negative for SC and neighboring endothelial-lined vessels.

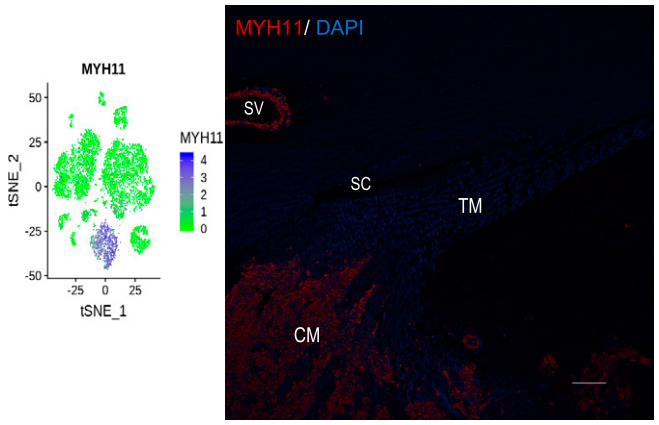

Fig. 5. Localization of smooth muscle cell cluster gene candidates using in situ hybridization of human eye sections. (*Left*) tSNE plot showing normalized MYH11 gene expression in each cell (blue dots). (*Right*) ISH-stained human eye section showing specific mRNA signal as red dot fluorescence of the MYH11 gene. The mRNA probe to MYH11 was predominantly confined to ciliary muscle. DAPI staining (blue) counterstains cell nuclei. Magnification, 20×. SV, scleral vessel. The scale in the tSNE plot shows the natural log-transformed scaled read counts. (Scale bar, 50 μm.)

Lastly, we were interested in looking at candidate markers for myelin-containing Schwann and resident macrophages and natural killer (NK) cells in the TM. For Schwann cells, we labeled human outflow tissues with two different antibodies raised against myelin-PLP, without specific staining (*SI Appendix*, Table S3). For NK cells and macrophages, we labeled human outflow tissue antibodies raised against DAP12 and LYVE1, respectively. Interestingly, LYVE1 staining was positive against some cells in the TM, with more prominent staining of the cells around the SC lumen and lymphatic vessels (Fig. 10*D*).

Discussion

The conventional outflow pathway is a complex tissue involved in maintaining IOP homeostasis. Cells that reside in the pathway have complementary roles to ensure faithful regulation of outflow resistance, and thus IOP. We used scRNAseq to generate an atlas of human conventional outflow cells to more accurately define their cellular roles based upon differential gene expression and tissue localization. The dataset was robust, being generated from eight individual samples from four human donors. These expression data more accurately and convincingly identify the various individual cell types, cell type-specific gene markers, and disease-related gene expression across the different cell types in the conventional outflow pathway. A major outcome of the present study was the identification of 12 different cell types in or adjacent to conventional outflow tissues. Importantly, we clearly found that there are two distinct "molecular types" of TM cells with related expression patterns. We also showed in human eyes the hybrid blood vascular/lymphatic character of SC, supporting mouse lineage tracing data. Finally, we demonstrated the utility of our dataset by localizing select glaucoma-related genes to specific cell populations in the outflow tract. These findings

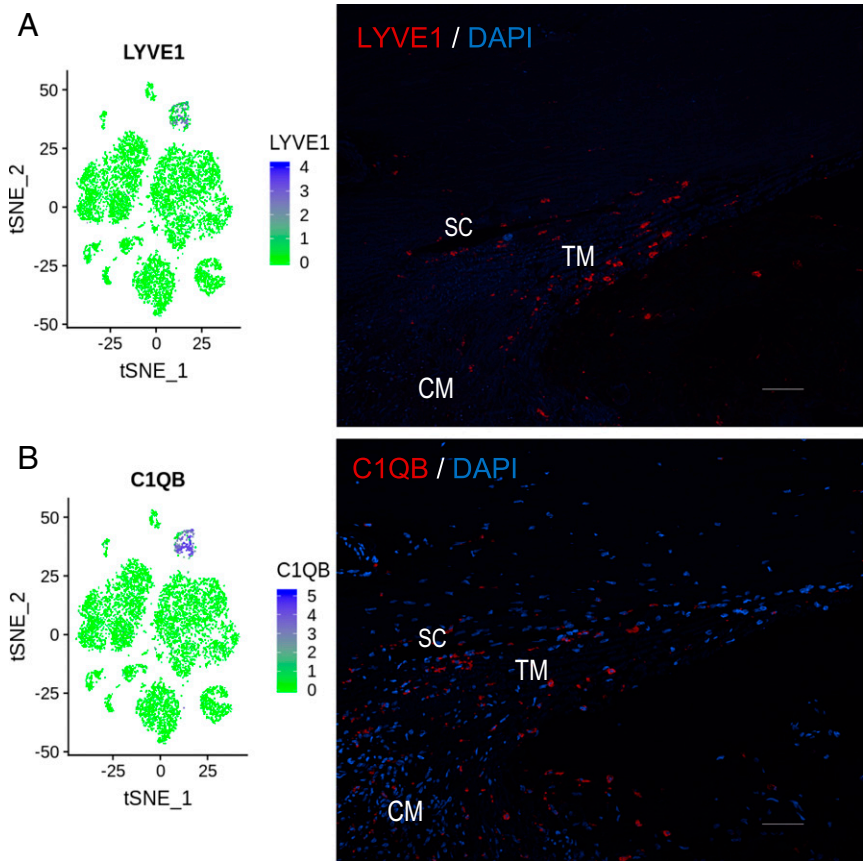

Fig. 6. Mapping of macrophage genes in human outflow tissues using in situ hybridization. (*Left*) A tSNE plot showing normalized gene expression in each cell (blue dots). (*Right*) An ISH-stained human eye section showing mRNA signal as red dot fluorescence. mRNA probes to LYVE1 (*A*) and C1QB (*B*) show that macrophages are present throughout the TM and ciliary muscle and around SC. DAPI staining (blue) counterstains cell nuclei. Magnification, 20×. The scale in the tSNE plots shows the intensity of the natural log-transformed scaled read counts. (Scale bars, 50 μm.)

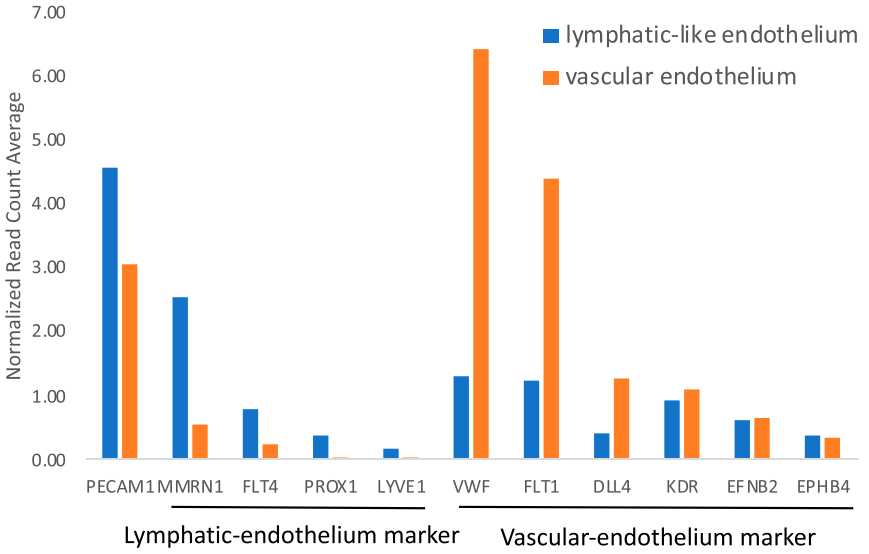

Fig. 7. Lymphatic and vascular marker expression in the scRNAseq outflow tissue transcriptome. Lymphatic-like endothelial cells express the pan-endothelial marker PECAM1 and also express higher levels of lymphatic endothelial cell markers MMRN1 and FLT4 than vascular endothelial cells but lower levels of vascular endothelial cell markers VWF and FLT1.

have only scratched the surface of this valuable and reliable dataset that can be used by conventional outflow researchers for years to come.

One of the major cell types identified was the Schwann cell-like cell cluster. Despite the abundance of this cell type in our single-cell samples, it was found not to be a major complement

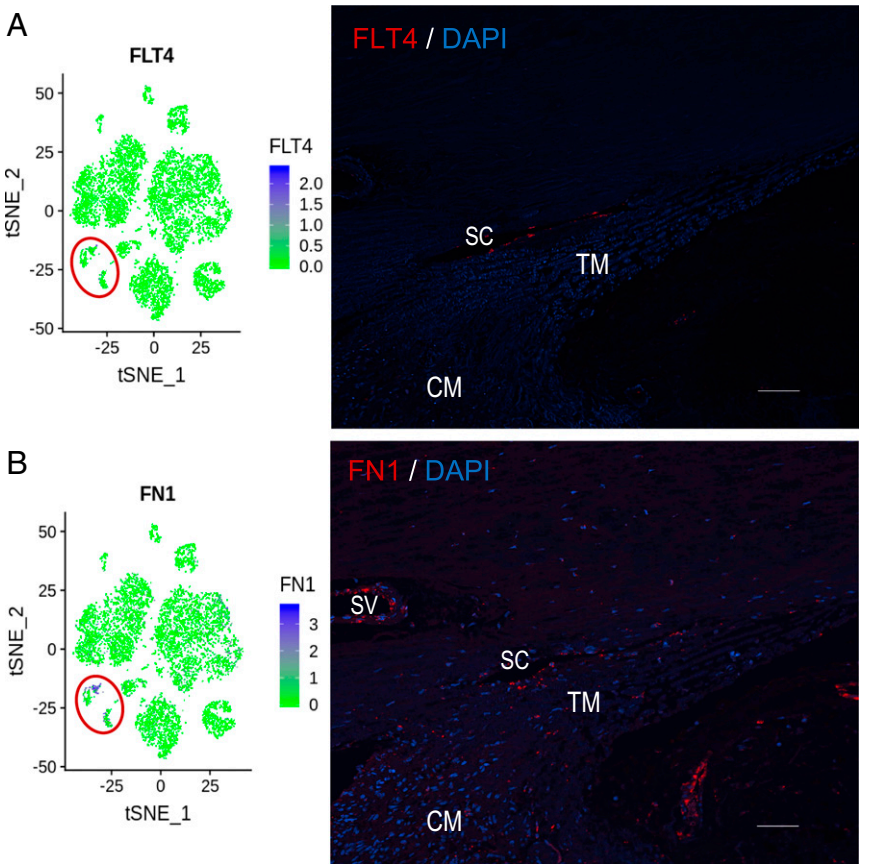

Fig. 8. Localization of lymphatic and vascular endothelial cell expression in human eye sections using in situ hybridization. (*Left*) A tSNE plot showing normalized gene expression in each cell (blue dots). (*Right*) A stained human eye section showing mRNA signal as red fluorescence. mRNA probes corresponding to FLT4 (*A*) and FN1 (*B*) were predominantly found in the SC region. FN1 was also localized more to JCT and other regions. DAPI staining (blue) counterstains cell nuclei. Magnification, 20×. The scale in the tSNE plots shows the intensity of natural log-transformed scaled read counts. The red circles in the tSNE plots highlight lymphatic–vascular endothelial cell clusters. (Scale bars, 50 μm.)

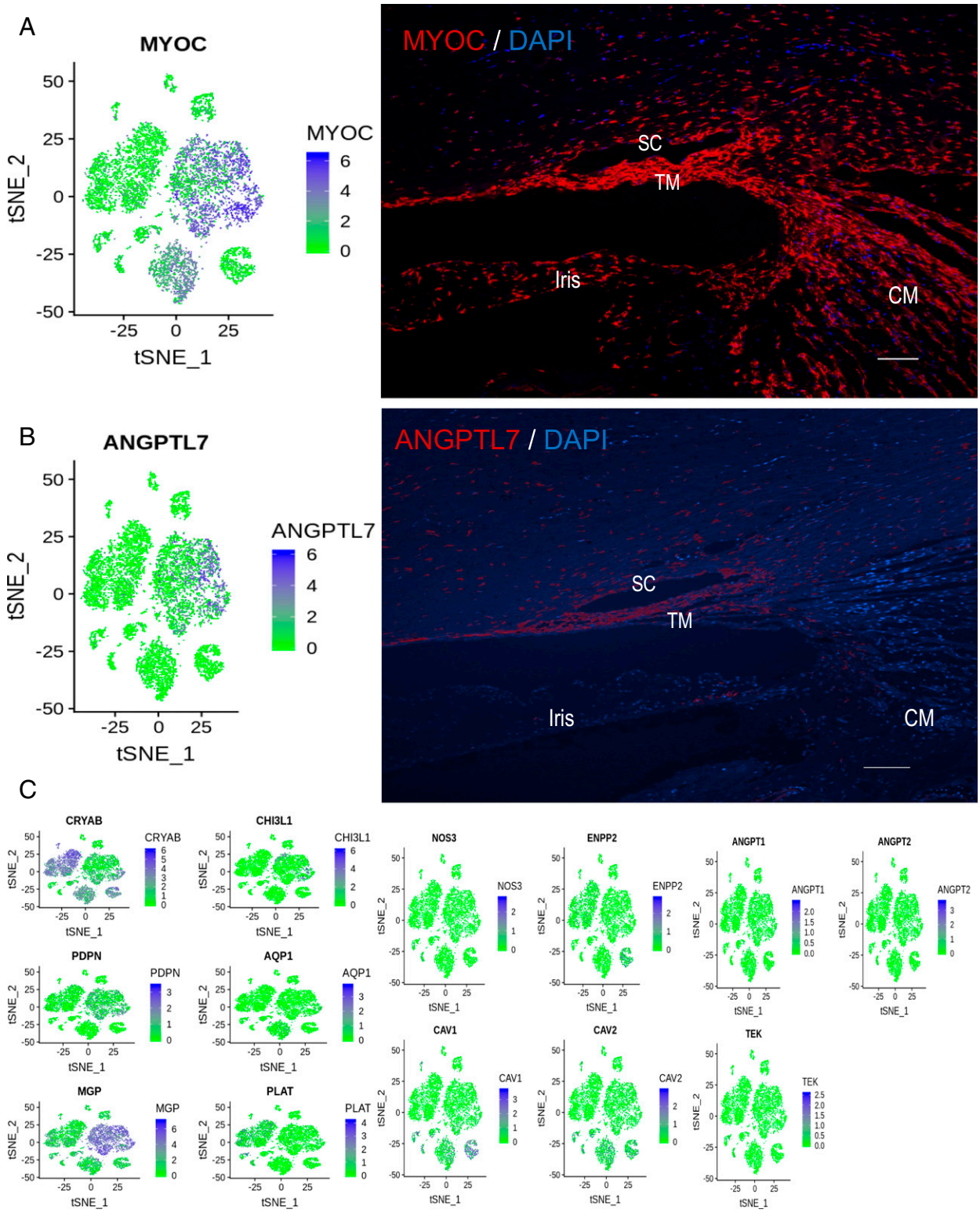

Fig. 9. Expression of glaucoma-related genes in cell clusters identified in scRNAseq from human outflow cells and in human tissue sections by in situ hybridization. (*Left*) tSNE plot of normalized expression of a glaucoma gene in each cell (blue dots). (*Right*) An ISH-stained human eye section showing mRNA signal as red dot fluorescence. (*A*) mRNA probes specific for MYOC localize strong expression throughout the TM, with lower expression in the ciliary muscle and surrounding tissues. (*B*) ANGPTL7 was confined to JCT and SC regions of the outflow tract in human eye sections. DAPI staining (blue) counterstains cell nuclei. Magnification, 10×. (*C*) tSNE plots with normalized expression of a glaucoma gene in each cell (blue dots). ENPP2, CAV1, CAV2, NOS3, ANGPT1, ANGPT2, TEK, CRYAB, CHI3L1, PDPN, AQP1, MGP, and PLAT gene expression is displayed. The scale in the tSNE plots shows the intensity of the natural log-transformed scaled read counts. (Scale bars, 100 μm.)

Table 1. Glaucoma-associated gene expression (average UMI) in different cell clusters

Gene	Lymphatic-like endothelium	Vascular endothelium	Pericyte	Smooth muscle cell	TM2 myofibroblast-like	TM1 fibroblast-like	Myelinating Schwann cell	Schwann cell-like	Melanocyte	Epithelium	T/NK cell	Macrophage
NOS3	0.42	0.60	0.05	0.00	0.01	0.01	0.00	0.00	0.01	0.00	0.04	0.00
ENPP2	0.00	0.10	0.03	0.03	0.02	0.07	0.53	0.69	1.60	0.00	0.02	0.05
CAV1	5.17	2.92	2.32	1.76	0.59	0.11	2.75	0.14	7.35	0.62	0.30	0.09
CAV2	2.14	2.09	1.62	1.40	0.41	0.27	1.31	0.09	1.79	0.86	0.08	0.04
ANGPT1	0.01	0.02	0.16	0.09	0.12	0.11	0.01	0.02	0.00	0.00	0.00	0.00
ANGPT2	0.13	0.59	0.33	0.02	0.05	0.07	0.08	0.06	0.04	0.03	0.09	0.01
TEK	0.84	0.62	0.04	0.00	0.01	0.01	0.01	0.00	0.00	0.00	0.00	0.00
CRYAB	1.77	1.35	8.20	15.66	14.03	3.52	70.56	50.57	33.77	4.24	1.32	1.59
CHI3L1	0.02	0.12	1.42	0.08	10.48	4.34	0.15	0.16	0.05	0.11	0.27	0.17
PDPN	0.12	0.06	0.10	0.12	2.67	2.02	0.24	0.68	0.04	0.04	0.15	0.07
AQP1	0.17	0.18	0.16	0.75	0.37	0.11	0.05	0.05	0.01	0.00	0.00	0.03
MGP	10.71	8.93	17.45	8.81	157.33	144.92	9.93	8.50	12.40	6.50	6.28	5.46
PLAT	12.78	2.68	0.28	0.10	0.34	0.49	1.34	2.80	0.31	0.77	0.08	0.02

For each gene, saturated yellow represents highest expression among molecularly defined cell types, saturated blue represents lowest expression, and intermediate shades of color represent intermediate expression.

of the TM proper. Our in situ hybridization results mapped this cluster primarily to scleral spur and ciliary muscle regions in human eye sections. These data are consistent with other studies showing the presence of nerves that innervate scleral spur cells or mechanosensory nerve endings in the scleral spur and ciliary muscle regions (8, 63–66). Electron micrographs of nerve terminals in the scleral spur show that the surface of such terminals is ensheathed by flat processes of Schwann cells (8, 66). The elastic fibers and nerve terminals of scleral spurs are directly continuous with elastic fibers of the TM and extend with the ECM of the TM (8, 64). Along this path, we found a few cells expressing these markers that extended into the TM (Fig. 2 and *SI Appendix*, Fig. S5), consistent with transmission electron microscopy data of human eyes (64).

Our results suggest that TM2, TM1, lymphatic-like, vascular endothelial cell, and macrophage cell clusters represent the primary components of the conventional outflow pathway corresponding to TM cells on beams/cribriform plates, JCT cells, SC endothelia, and macrophages throughout. While the candidate genes RSPO2 and RSPO4 were primarily found in the TM2-myofibroblast cell cluster, in situ hybridization demonstrated a broader distribution across the TM, with RSPO4 being more restricted to the TM than RSPO2. Immunolabeling of RSPO2 protein confirmed in situ hybridization results, showing some preferential expression in TM cells. RSPO2 and RSPO4 are secreted proteins that enhance Wnt signaling, a known regulatory pathway of outflow resistance and IOP (67, 68). While also being expressed at low levels in neighboring tissues, the TM1-fibroblast cell cluster candidate genes DCN and PDGFRA are preferentially localized to the JCT region of the outflow tract, a region critical for generating outflow resistance (7). TM cells in the JCT region display a fibroblast and smooth muscle-like phenotype and modulate ECM turnover and repair (7). DCN encodes decorin, which is a proteoglycan that regulates ECM deposition and is an antagonist of transforming growth factor β (TGFβ) and connective tissue growth factor (CTGF) pathways. Diminished decorin levels have been observed in aqueous humor of glaucoma patients (69) and decorin treatment lowers IOP and retinal ganglion cell loss in animals models (70). Finally, the lymphatic-like endothelial cell cluster expressed markers of both vascular and lymphatic endothelial cells, suggesting SC as a unique vessel (43). These primary data in human eyes support findings of mouse lineage tracing studies (43). Some markers, like DCN and FN1, although expressed at higher levels in one cluster, were also expressed at low levels in other cell clusters. We only performed RNAscope to show their mRNA expression and chose not to examine samples of human eye sections for decorin or fibronectin protein because both have been previously shown to have widespread expression in the conventional outflow tract (71). The select group of glaucoma-related genes we tested was found distributed to different outflow cell types in the conventional outflow pathway. For example, MYOC, ANGPTL7, PDPN, CHI3L1, and ANGPT1 were highly expressed in TM1 and TM2 cell clusters, while CAV1, CAV2, NOS3, Tie2 (TEK), PLAT, and ANGPT2 were highly expressed in lymphatic-like and vascular endothelial cell clusters (i.e., SC).

Unconventional outflow pathway structures which include ciliary muscle and scleral spur cells were represented in our atlas by smooth muscle cell and scleral spur/Schwann cell-like cell clusters. One of the candidate genes, TAGLN, mapped to TM2 and smooth muscle clusters, appearing expressed at higher levels in ciliary muscle compared with TM by in situ hybridization. TAGLN encodes transgelin, which is an actin-binding protein that is ubiquitously expressed in vascular and visceral smooth muscle cells (72). These data emphasize the important contractile connection between the ciliary muscle and the TM. Unexpectedly, autotaxin (encoded by ENPP2), which has been shown to be elevated in aqueous humor of glaucoma patients (49, 50), was expressed in scleral spur/Schwann cell-like cluster and melanocyte cell clusters but not in TM1 or TM2. This is in contrast to previous reports finding autotaxin protein in human TM specimens (73). This highlights a limitation of current single-cell technology, which is not sensitive enough to detect all of the mRNA molecules in the cell (74). Very often mRNA of genes expressed at low levels is not detected in every cell of the same cell type. This phenomenon is called "dropout," which is important to keep in mind when interpreting the biology of scRNAseq data.

One of the important functions of TM cells is to clear debris delivered via aqueous humor flow as it moves across ocular structures in the posterior and anterior chambers. TM cells in the uveal/corneoscleral meshwork have scavenger receptors and work as filters to clear cellular debris by phagocytosis before it reaches the resistance-generating JCT region (15–17). It appears that TM cells do not work alone but coordinate activities with resident macrophages as it has been observed in smooth muscle-containing blood vessels (75). Consistent with this idea, our results map macrophage candidate genes (LYVE1, C1QB, and TYROBP) abundantly throughout the conventional outflow tract, from the inner TM to the outer wall of SC and distal vessels, suggesting a homeostatic function in outflow regulation.

In all of our conventional outflow samples, we consistently identified cells that mapped to clusters including the T/NK cell, epithelium, melanocyte, and pericyte (*SI Appendix*, Fig. S9). We

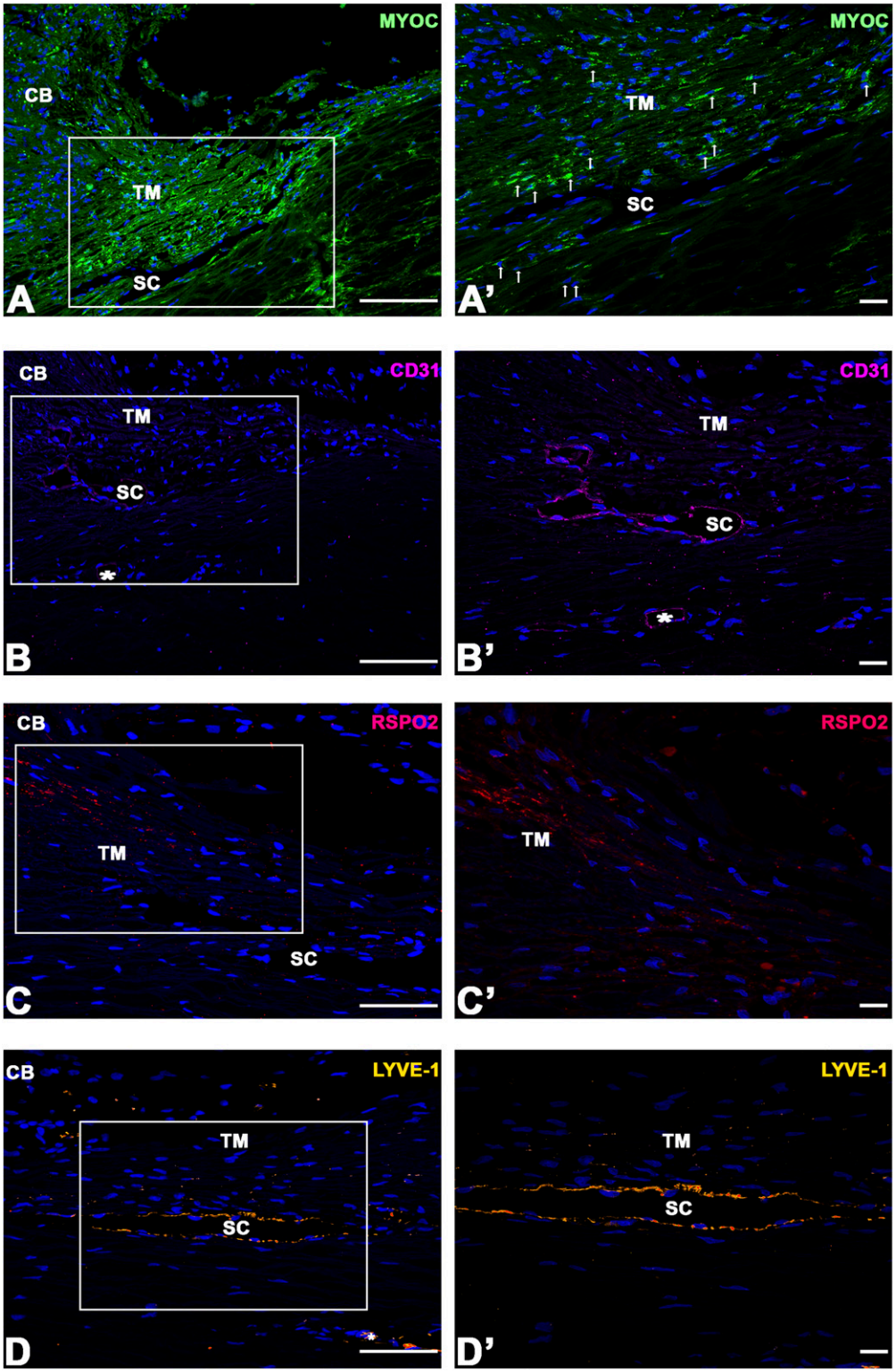

Fig. 10. Immunolocalization of protein products of gene cluster markers in conventional outflow tissues from human eye sections. (*Left*) Low-magnification view of conventional outflow structures in cross-section. Areas of interest are indicated by a white box, which corresponds to a higher-magnification image (*Right*). (*A*) Strong TM labeling of the glaucoma gene product myocilin. Arrows point to cells showing characteristic perinuclear labeling. (*B*) Staining for the vascular endothelial cluster marker CD31 (PECAM1), which positively labels Schlemm's canal and a scleral vessel (asterisks). (*C*) The TM2 gene cluster candidate R-spondin-2 displaying preferential labeling in the uveal/corneoscleral region of the conventional tract. (*D*) The macrophage cluster marker lymphatic vessel endothelial hyaluronan receptor 1 showing predominant labeling of cells surrounding Schlemm's canal and a lymphatic vessel in sclera (asterisk). All sections were counterstained with DAPI to show the location of cell nuclei. CB, ciliary body. (Scale bars, 100 μm [*Left*] and 20 μm [*Right*].)

speculate that they may be contaminants introduced during the dissection or from neighboring tissues. Interestingly, while T/NK, epithelium, and pericyte were represented by a few cells, a large number of cells appeared in the melanocyte cluster.

In conclusion, using scRNAseq, we have identified 12 distinct cell types in and around the human conventional outflow pathway, emphasizing the diversity of cells that participate in the regulation of outflow function and thus IOP control. In addition to documenting the unique lymphatic/blood vascular expression profile of SC, our findings also settle the long-standing controversy as to the number of TM cell "types" in the conventional outflow pathway, finding two. These data provide essential information for identity confirmation of TM and SC cells in culture, designing cell-specific promoters, and testing druggable targets for novel glaucoma therapies.

Materials and Methods

Human Eye Tissue Procurement and Dissection. Human donor eyes (four normal donors) were obtained from the Lions Eye Institute for Transplant and Research (Tampa, FL) and Miracles in Sight (Winston-Salem, NC) in moist chambers on ice (*SI Appendix*, Table S1). For dissecting the trabecular meshwork, a blunt dissection approach was used (25). The TM tissue was placed in digestion buffer containing 5 mg collagenase A dissolved in human albumin. Hematoxylin and eosin staining of TM tissue before and after dissection is shown in *SI Appendix*, Fig. S1. (A detailed protocol is in *SI Appendix, Text*.)

Sample Preparation (Cell Dissociation and Viability Test). The TM tissues in digestion buffer were incubated for 2 to 3 h at 37 °C and 5% CO_2, and shaken every 20 min. At the end of incubation, TM single-cell suspension and tissue debris were mixed with Dulbecco's modified Eagle's medium and filtered through a 70-μm filter to get the maximum number of cells after tissue digestion. The single-cell solution was centrifuged at 1,000 × *g* for 10 min. The single-cell pellet was resuspended in phosphate-buffered saline (PBS) with 0.04% bovine serum albumin (BSA). Cell viability was determined by the NucleoCounter NC-250 automated cell analyzer (details are in *SI Appendix, Text*).

Single-Cell RNA Sequencing and Read Mapping. Single cells suspended in PBS with 0.04% BSA were loaded on a Chromium Single Cell Instrument (10x Genomics). RNAseq libraries were prepared using the Chromium Single Cell 3′ Library, Gel Beads & Multiplex Kit (10x Genomics). Paired-end sequencing was performed on an Illumina NextSeq 500. (A detailed protocol is in *SI Appendix, Text*.)

Data Analysis. We mainly used the Seurat 2.3 software package developed by the Satija laboratory for the single-cell data analysis (details are in *SI Appendix, Text*). The similarity or dissimilarity among the identified cell types was examined by hierarchical clustering using Euclidean distance and complete linkage algorithm in R (R Core Team 2017, https://www.r-project.org/).

Data Availability. Raw data files have been deposited in the Sequence Read Archive of the National Center for Biotechnology Information with accession no. PRJNA616025.

In Situ Hybridization Using RNAscope and Immunohistochemistry. The expression pattern of TM single-cell cluster-specific gene expression in human donor eyes was determined by in situ hybridization using RNAscope according to the manufacturer's specifications (Advanced Cell Diagnostics) and standard immunohistochemistry protocols. (A detailed protocol is in *SI Appendix, Text*.)

ACKNOWLEDGMENTS. We thank Joshua R. Sanes and Tavé van Zyl for sharing results of their parallel study prior to submission. This work was supported by NIH Grants EY022359 and EY028608.

1. M. O. Gordon *et al*., The Ocular Hypertension Treatment Study: Baseline factors that predict the onset of primary open-angle glaucoma. *Arch. Ophthalmol.* **120**, 714–720; discussion 829–830 (2002).
2. The AGIS Investigators, The Advanced Glaucoma Intervention Study (AGIS): 7. The relationship between control of intraocular pressure and visual field deterioration. *Am. J. Ophthalmol.* **130**, 429–440 (2000).
3. A. Heijl *et al*.; Early Manifest Glaucoma Trial Group, Reduction of intraocular pressure and glaucoma progression: Results from the Early Manifest Glaucoma Trial. *Arch. Ophthalmol.* **120**, 1268–1279 (2002).
4. Collaborative Normal-Tension Glaucoma Study Group, Comparison of glaucomatous progression between untreated patients with normal-tension glaucoma and patients with therapeutically reduced intraocular pressures. *Am. J. Ophthalmol.* **126**, 487–497 (1998).
5. I.-H. Pang, A. F. Clark, "Chapter 3—IOP as a target—Inflow and outflow pathways" in *Ocular Therapeutics*, T. Yorio, A. F. Clark, M. B. Wax, Eds. (Academic Press, London, 2008), pp. 45–67.
6. C. M. Adams *et al*., Glaucoma—Next generation therapeutics: Impossible to possible. *Pharm. Res.* **36**, 25 (2018).
7. W. D. Stamer, A. F. Clark, The many faces of the trabecular meshwork cell. *Exp. Eye Res.* **158**, 112–123 (2017).
8. E. R. Tamm, The trabecular meshwork outflow pathways: Structural and functional aspects. *Exp. Eye Res.* **88**, 648–655 (2009).
9. B. E. Klein, R. Klein, K. L. Linton, Intraocular pressure in an American community. The Beaver Dam Eye Study. *Invest. Ophthalmol. Vis. Sci.* **33**, 2224–2228 (1992).
10. R. David, L. Zangwill, D. Stone, Y. Yassur, Epidemiology of intraocular pressure in a population screened for glaucoma. *Br. J. Ophthalmol.* **71**, 766–771 (1987).
11. B. T. Gabelt, P. L. Kaufman, Changes in aqueous humor dynamics with age and glaucoma. *Prog. Retin. Eye Res.* **24**, 612–637 (2005).
12. W. D. Stamer, T. S. Acott, Current understanding of conventional outflow dysfunction in glaucoma. *Curr. Opin. Ophthalmol.* **23**, 135–143 (2012).
13. B. J. Tripathi, R. C. Tripathi, Neural crest origin of human trabecular meshwork and its implications for the pathogenesis of glaucoma. *Am. J. Ophthalmol.* **107**, 583–590 (1989).
14. M. A. Shuman, J. R. Polansky, C. Merkel, J. A. Alvarado, Tissue plasminogen activator in cultured human trabecular meshwork cells. Predominance of enzyme over plasminogen activator inhibitor. *Invest. Ophthalmol. Vis. Sci.* **29**, 401–405 (1988).
15. D. H. Johnson, T. M. Richardson, D. L. Epstein, Trabecular meshwork recovery after phagocytic challenge. *Curr. Eye Res.* **8**, 1121–1130 (1989).
16. D. L. Epstein, T. F. Freddo, P. J. Anderson, M. M. Patterson, S. Bassett-Chu, Experimental obstruction to aqueous outflow by pigment particles in living monkeys. *Invest. Ophthalmol. Vis. Sci.* **27**, 387–395 (1986).
17. D. A. Samuelson, K. N. Gelatt, G. G. Gum, Kinetics of phagocytosis in the normal canine iridocorneal angle. *Am. J. Vet. Res.* **45**, 2359–2366 (1984).
18. M. G. Lynch, J. S. Peeler, R. H. Brown, J. Y. Niederkorn, Expression of HLA class I and II antigens on cells of the human trabecular meshwork. *Ophthalmology* **94**, 851–857 (1987).
19. A. S. Shifera *et al*., Constitutive secretion of chemokines by cultured human trabecular meshwork cells. *Exp. Eye Res.* **91**, 42–47 (2010).
20. B. Tian, B. T. Gabelt, B. Geiger, P. L. Kaufman, The role of the actomyosin system in regulating trabecular fluid outflow. *Exp. Eye Res.* **88**, 713–717 (2009).
21. D. R. Overby *et al*., The structure of the trabecular meshwork, its connections to the ciliary muscle, and the effect of pilocarpine on outflow facility in mice. *Invest. Ophthalmol. Vis. Sci.* **55**, 3727–3736 (2014).
22. R. J. Wordinger, A. F. Clark, Effects of glucocorticoids on the trabecular meshwork: Towards a better understanding of glaucoma. *Prog. Retin. Eye Res.* **18**, 629–667 (1999).
23. K. E. Keller, M. Aga, J. M. Bradley, M. J. Kelley, T. S. Acott, Extracellular matrix turnover and outflow resistance. *Exp. Eye Res.* **88**, 676–682 (2009).
24. P. V. Rao, P. P. Pattabiraman, C. Kopczynski, Role of the Rho GTPase/Rho kinase signaling pathway in pathogenesis and treatment of glaucoma: Bench to bedside research. *Exp. Eye Res.* **158**, 23–32 (2017).
25. K. E. Keller *et al*., Consensus recommendations for trabecular meshwork cell isolation, characterization and culture. *Exp. Eye Res.* **171**, 164–173 (2018).
26. P. Gonzalez, M. Caballero, P. B. Liton, W. D. Stamer, D. L. Epstein, Expression analysis of the matrix GLA protein and VE-cadherin gene promoters in the outflow pathway. *Invest. Ophthalmol. Vis. Sci.* **45**, 1389–1395 (2004).
27. P. B. Liton *et al*., Specific targeting of gene expression to a subset of human trabecular meshwork cells using the chitinase 3-like 1 promoter. *Invest. Ophthalmol. Vis. Sci.* **46**, 183–190 (2005).
28. P. Asokan, R. N. Mitra, R. Periasamy, Z. Han, T. Borrás, A naturally fluorescent Mgp transgenic mouse for angiogenesis and glaucoma longitudinal studies. *Invest. Ophthalmol. Vis. Sci.* **59**, 746–756 (2018).
29. J. R. Polansky, D. J. Fauss, C. C. Zimmerman, Regulation of TIGR/MYOC gene expression in human trabecular meshwork cells. *Eye (Lond.)* **14**, 503–514 (2000).
30. P. B. Liton, C. Luna, P. Challa, D. L. Epstein, P. Gonzalez, Genome-wide expression profile of human trabecular meshwork cultured cells, nonglaucomatous and primary open angle glaucoma tissue. *Mol. Vis.* **12**, 774–790 (2006).
31. Y. Liu *et al*., Gene expression profile in human trabecular meshwork from patients with primary open-angle glaucoma. *Invest. Ophthalmol. Vis. Sci.* **54**, 6382–6389 (2013).
32. M. K. Wirtz, J. R. Samples, H. Xu, T. Severson, T. S. Acott, Expression profile and genome location of cDNA clones from an infant human trabecular meshwork cell library. *Invest. Ophthalmol. Vis. Sci.* **43**, 3698–3704 (2002).
33. P. Sathiyanathan, C. Y. Tay, L. W. Stanton, Transcriptome analysis for the identification of cellular markers related to trabecular meshwork differentiation. *BMC Genomics* **18**, 383 (2017).
34. M. U. Carnes, R. R. Allingham, A. Ashley-Koch, M. A. Hauser, Transcriptome analysis of adult and fetal trabecular meshwork, cornea, and ciliary body tissues by RNA sequencing. *Exp. Eye Res.* **167**, 91–99 (2018).

35. S. I. Tomarev, G. Wistow, V. Raymond, S. Dubois, I. Malyukova, Gene expression profile of the human trabecular meshwork: NEIBank sequence tag analysis. *Invest. Ophthalmol. Vis. Sci.* **44**, 2588–2596 (2003).
36. A. M. Klein *et al*., Droplet barcoding for single-cell transcriptomics applied to embryonic stem cells. *Cell* **161**, 1187–1201 (2015).
37. D. A. Jaitin *et al*., Massively parallel single-cell RNA-seq for marker-free decomposition of tissues into cell types. *Science* **343**, 776–779 (2014).
38. E. Z. Macosko *et al*., Highly parallel genome-wide expression profiling of individual cells using nanoliter droplets. *Cell* **161**, 1202–1214 (2015).
39. B. A. Rheaume *et al*., Single cell transcriptome profiling of retinal ganglion cells identifies cellular subtypes. *Nat. Commun.* **9**, 2759 (2018).
40. Y. R. Peng *et al*., Molecular classification and comparative taxonomics of foveal and peripheral cells in primate retina. *Cell* **176**, 1222–1237.e22 (2019).
41. N. Kaplan *et al*., Single-cell RNA transcriptome helps define the limbal/corneal epithelial stem/early transit amplifying cells and how autophagy affects this population. *Invest. Ophthalmol. Vis. Sci.* **60**, 3570–3583 (2019).
42. W. D. Stamer *et al*., Biomechanics of Schlemm's canal endothelium and intraocular pressure reduction. *Prog. Retin. Eye Res.* **44**, 86–98 (2015).
43. K. Kizhatil, M. Ryan, J. K. Marchant, S. Henrich, S. W. John, Schlemm's canal is a unique vessel with a combination of blood vascular and lymphatic phenotypes that forms by a novel developmental process. *PLoS Biol.* **12**, e1001912 (2014).
44. E. M. Stone *et al*., Identification of a gene that causes primary open angle glaucoma. *Science* **275**, 668–670 (1997).
45. J. Kuchtey *et al*., Angiopoietin-like 7 secretion is induced by glaucoma stimuli and its concentration is elevated in glaucomatous aqueous humor. *Invest. Ophthalmol. Vis. Sci.* **49**, 3438–3448 (2008).
46. N. Comes, L. K. Buie, T. Borrás, Evidence for a role of angiopoietin-like 7 (ANGPTL7) in extracellular matrix formation of the human trabecular meshwork: Implications for glaucoma. *Genes Cells* **16**, 243–259 (2011).
47. M. Aga *et al*., Differential effects of caveolin-1 and -2 knockdown on aqueous outflow and altered extracellular matrix turnover in caveolin-silenced trabecular meshwork cells. *Invest. Ophthalmol. Vis. Sci.* **55**, 5497–5509 (2014).
48. S. J. Loomis *et al*., Association of CAV1/CAV2 genomic variants with primary open-angle glaucoma overall and by gender and pattern of visual field loss. *Ophthalmology* **121**, 508–516 (2014).
49. L. T. Y. Ho *et al*., Role of the autotaxin-lysophosphatidic acid axis in glaucoma, aqueous humor drainage and fibrogenic activity. *Biochim. Biophys. Acta Mol. Basis Dis.* **1866**, 165560 (2020).
50. M. Honjo *et al*., Autotaxin-lysophosphatidic acid pathway in intraocular pressure regulation and glaucoma subtypes. *Invest. Ophthalmol. Vis. Sci.* **59**, 693–701 (2018).
51. P. Iyer *et al*., Autotaxin-lysophosphatidic acid axis is a novel molecular target for lowering intraocular pressure. *PLoS One* **7**, e42627 (2012).
52. C. Gambacorti-Passerini *et al*., Mapping of HLA class I binding motifs in forty-four fusion proteins involved in human cancers. *Clin. Cancer Res.* **3**, 675–683 (1997).
53. J. F. Logan *et al*., Evidence for association of endothelial nitric oxide synthase gene in subjects with glaucoma and a history of migraine. *Invest. Ophthalmol. Vis. Sci.* **46**, 3221–3226 (2005).
54. K. Polak *et al*., Altered nitric oxide system in patients with open-angle glaucoma. *Arch. Ophthalmol.* **125**, 494–498 (2007).
55. W. A. Emam *et al*., Endothelial nitric oxide synthase polymorphisms and susceptibility to high-tension primary open-angle glaucoma in an Egyptian cohort. *Mol. Vis.* **20**, 804–811 (2014).
56. H. Choquet *et al*., A large multi-ethnic genome-wide association study identifies novel genetic loci for intraocular pressure. *Nat. Commun.* **8**, 2108 (2017).
57. M. Kabra *et al*., Angiopoietin receptor TEK interacts with CYP1B1 in primary congenital glaucoma. *Hum. Genet.* **136**, 941–949 (2017).
58. A. P. Khawaja *et al*.; UK Biobank Eye and Vision Consortium; NEIGHBORHOOD Consortium, Genome-wide analyses identify 68 new loci associated with intraocular pressure and improve risk prediction for primary open-angle glaucoma. *Nat. Genet.* **50**, 778–782 (2018).
59. J. Kim *et al*., Impaired angiopoietin/Tie2 signaling compromises Schlemm's canal integrity and induces glaucoma. *J. Clin. Invest.* **127**, 3877–3896 (2017).
60. B. R. Thomson *et al*., A lymphatic defect causes ocular hypertension and glaucoma in mice. *J. Clin. Invest.* **124**, 4320–4324 (2014).
61. A. Siegner, C. A. May, U. W. Welge-Lüssen, H. Bloemendal, E. Lütjen-Drecoll, Alpha B-crystallin in the primate ciliary muscle and trabecular meshwork. *Eur. J. Cell Biol.* **71**, 165–169 (1996).
62. Y. Watanabe, T. Hamanaka, T. Takemura, A. Murakami, Involvement of platelet coagulation and inflammation in the endothelium of Schlemm's canal. *Invest. Ophthalmol. Vis. Sci.* **51**, 277–283 (2010).
63. G. L. Ruskell, The source of nerve fibres of the trabeculae and adjacent structures in monkey eyes. *Exp. Eye Res.* **23**, 449–459 (1976).
64. J. M. Selbach, J. Gottanka, M. Wittmann, E. Lütjen-Drecoll, Efferent and afferent innervation of primate trabecular meshwork and scleral spur. *Invest. Ophthalmol. Vis. Sci.* **41**, 2184–2191 (2000).
65. E. R. Tamm, T. A. Koch, B. Mayer, F. H. Stefani, E. Lütjen-Drecoll, Innervation of myofibroblast-like scleral spur cells in human monkey eyes. *Invest. Ophthalmol. Vis. Sci.* **36**, 1633–1644 (1995).
66. E. R. Tamm, C. Flügel, F. H. Stefani, E. Lütjen-Drecoll, Nerve endings with structural characteristics of mechanoreceptors in the human scleral spur. *Invest. Ophthalmol. Vis. Sci.* **35**, 1157–1166 (1994).
67. W. H. Wang *et al*., Increased expression of the WNT antagonist sFRP-1 in glaucoma elevates intraocular pressure. *J. Clin. Invest.* **118**, 1056–1064 (2008).
68. H. C. Webber, J. Y. Bermudez, J. C. Millar, W. Mao, A. F. Clark, The role of Wnt/β-catenin signaling and K-cadherin in the regulation of intraocular pressure. *Invest. Ophthalmol. Vis. Sci.* **59**, 1454–1466 (2018).
69. S. NikhalaShree *et al*., Lowered decorin with aberrant extracellular matrix remodeling in aqueous humor and Tenon's tissue from primary glaucoma patients. *Invest. Ophthalmol. Vis. Sci.* **60**, 4661–4669 (2019).
70. L. J. Hill *et al*., Decorin reduces intraocular pressure and retinal ganglion cell loss in rodents through fibrolysis of the scarred trabecular meshwork. *Invest. Ophthalmol. Vis. Sci.* **56**, 3743–3757 (2015).
71. T. S. Acott, M. J. Kelley, Extracellular matrix in the trabecular meshwork. *Exp. Eye Res.* **86**, 543–561 (2008).
72. J. L. Duband, M. Gimona, M. Scatena, S. Sartore, J. V. Small, Calponin and SM 22 as differentiation markers of smooth muscle: Spatiotemporal distribution during avian embryonic development. *Differentiation* **55**, 1–11 (1993).
73. M. Honjo *et al*., Role of the autotaxin-LPA pathway in dexamethasone-induced fibrotic responses and extracellular matrix production in human trabecular meshwork cells. *Invest. Ophthalmol. Vis. Sci.* **59**, 21–30 (2018).
74. S. Tracy, G. C. Yuan, R. Dries, RESCUE: Imputing dropout events in single-cell RNA-sequencing data. *BMC Bioinformatics* **20**, 388 (2019).
75. H. Y. Lim *et al*., Hyaluronan receptor LYVE-1-expressing macrophages maintain arterial tone through hyaluronan-mediated regulation of smooth muscle cell collagen. *Immunity* **49**, 326–341.e7 (2018).